

# Seasonal climate summary southern hemisphere (autumn 2009): signs of an El Niño in the Pacific

**Elise Chandler**

National Climate Centre, Bureau of Meteorology, Australia

(Manuscript received November 2009)

Southern hemisphere circulation patterns and associated anomalies for the austral autumn 2009 are reviewed, with emphasis given to Pacific Basin climate indicators and Australian rainfall and temperature patterns. Autumn 2009 saw neutral or near-neutral conditions in the Pacific following from the La Niña conditions experienced since late 2008. By the end of May 2009, the equatorial Pacific showed consistent warming, and the Southern Oscillation Index (SOI) fell, reaching  $-5.1$  in May. In the Indian Ocean, a positive Indian Ocean Dipole sea-surface temperature pattern started to establish itself during May. In the Australian region, autumn was drier than normal, with maximum temperatures above average over most of Australia.

## Introduction

This summary reviews southern hemisphere climate patterns acting around Australia and the southern hemisphere for the austral autumn (March to May) 2009. Particular attention is given to the Australasian and Pacific regions. The main sources of information used for this summary were analyses prepared by the Australian Bureau of Meteorology and the Centre for Australian Weather and Climate Research (CAWCR). This article begins with discussion at the largest spatial scales of climate variability and ends with a more detailed analysis of the Australian region.

## ENSO and Pacific Basin climate indices

### The Troup Southern Oscillation Index

The Troup Southern Oscillation Index (SOI) for the period January 2005 to May 2009 is shown in Fig. 1, together with a five-month weighted moving average. The SOI<sup>1</sup> is derived

from the mean sea-level pressure (MSLP) at both Darwin and Tahiti, and sustained values can be used as an indicator of El Niño–Southern Oscillation (ENSO) events.

The SOI remained positive through summer 2008-09 and early autumn, with a maximum monthly value of  $+14.8$  in February. SOI values then fluctuated somewhat around a falling trend during autumn ( $+0.2$  in March,  $+8.6$  in April,  $-5.1$  in May), consistent with a return to neutral ENSO conditions. The average SOI for autumn was  $+1.2$ , much lower than the summer average of  $+12.5$  (Mullen 2009). The general downward trend in the SOI through the season was mostly due to a moderate fall in MSLP at Tahiti from April to May (monthly MSLP anomalies<sup>2</sup> at Tahiti were  $+0.9$  hPa in March,  $+0.8$  hPa in April,  $-1.0$  hPa in May), counteracted somewhat by falling MSLP at Darwin (monthly anomalies there were  $+0.9$  hPa in March,  $-0.2$  hPa in April,  $-0.4$  hPa in May). The May MSLP anomaly at Tahiti ( $-1.0$  hPa) was the first negative value in its monthly time series since September 2007.

### Multivariate ENSO index

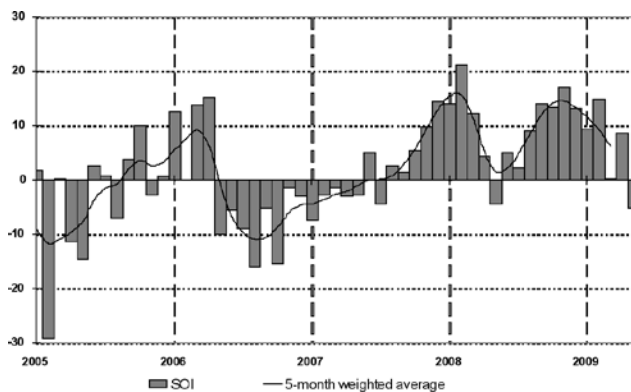
The US Climate Diagnostics Center's Multivariate ENSO Index (MEI) is derived from a number of atmospheric and oceanic parameters typically associated with ENSO, and calculated as a bimonthly value (Wolter and Timlin 1993, 1998).

<sup>1</sup> The Troup SOI (Troup 1965) used in this article is ten times the standardised monthly anomaly of the difference in MSLP between Tahiti and Darwin. The standardisation calculation is based on a sixty-year climatology (1933-1992). The Tahiti MSLP data are provided by Météo France interregional direction for French Polynesia. Monthly SOI data, together with contributing monthly MSLP data from Tahiti and Darwin, are obtained from <http://www.bom.gov.au/climate/current/soihtm1.shtml>.

Corresponding author address: Elise Chandler, National Climate Centre, Bureau of Meteorology, GPO Box 1289, Melbourne, Vic. 3001, Australia. Email: [e.chandler@bom.gov.au](mailto:e.chandler@bom.gov.au)

<sup>2</sup> As with the SOI, calculated with respect to the base period 1933-1992.

Fig. 1 Monthly Southern Oscillation Index, from January 2005 to May 2009. Mean and standard deviations used in the computation of the SOI are based on the period 1933-1992.



The index is a standardised anomaly index, with positive (negative) values indicative of El Niño (La Niña). The March-April value of the MEI was  $-0.191$  (rank 22 of 59), while the April-May value was  $+0.344$  (rank 37 of 59). While these values can be considered 'neutral' (Climate Diagnostics Center 2009a,b), a rising trend was evident and the April-May value was the first positive value since June-July 2008. This trend in the MEI, together with the trend in the SOI, was indicative of a possible transition to El Niño conditions.

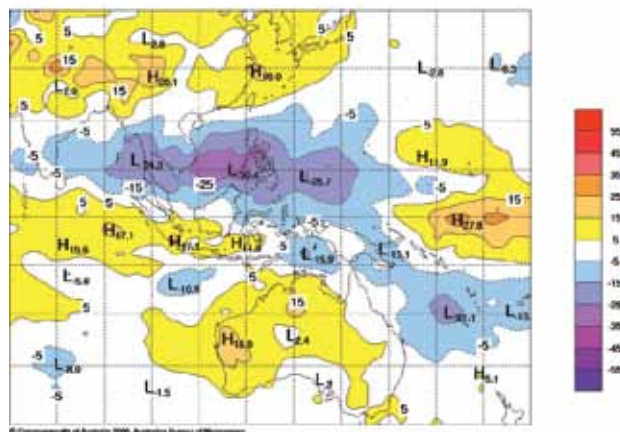
#### Outgoing long-wave radiation

Outgoing long-wave radiation (OLR) over the equatorial Pacific is a good measure of tropical deep convection, with increases in OLR indicating decreases in convection and vice versa. Convection in the equatorial region centred about the date-line is sensitive to changes in the Walker circulation. Studies have shown that during El Niño events, OLR is generally reduced (i.e., convection is generally enhanced) along the equator, particularly near and east of the date-line. During La Niña events, OLR is often increased (i.e. convection is suppressed) over the same region (Vincent et al. 1998).

The spatial pattern of seasonal OLR anomalies for autumn is shown in Fig. 2. Positive anomalies are present in the equatorial Pacific near the date-line, representing suppressed convection and rainfall. In the western equatorial Pacific there are negative anomalies present, lying to the east and north of the Australian continent. Much of Australia shows positive OLR anomalies for autumn with normal conditions over eastern coastal regions. This is consistent with the near-normal rainfall experienced in eastern Australia and drier than normal conditions over the rest of the country (Fig. 16).

The spatial pattern of seasonal OLR has some La Niña characteristics, such as the positive OLR near the date-line and the surrounding negative anomalies. This represents a continuation of the residual La Niña conditions evident

Fig. 2 Anomalies of OLR for autumn 2009 ( $W m^{-2}$ ). Base period 1979 to 1998. The mapped region extends from  $40^{\circ}S$  to  $40^{\circ}N$  and  $70^{\circ}E$  to  $180^{\circ}E$ .



over summer 2008-09, although at reduced amplitude: the maximum anomalous OLR in the vicinity of the date-line was  $+40.1 W m^{-2}$  in summer (not shown), falling to  $+27.8 W m^{-2}$  in autumn. The strength of this dipole signal declined during autumn, with the OLR returning to near neutral conditions. Maximum anomalous monthly OLR in the vicinity of the date-line fell from  $+40.4 W m^{-2}$  in March to  $+29.3 W m^{-2}$  in May, with an even lower value of  $+24.3 W m^{-2}$  in April.

#### Zonal winds across the equatorial Pacific

A Hovmöller plot of 850 hPa zonal winds across the equator from December 2008 to June 2009 is shown in Fig. 3 (obtained from CAWCR). The plot shows stronger than normal equatorial trade winds in the central and western Pacific through late summer and early autumn, although these weakened substantially through March. A burst of stronger easterly flow appeared again in mid-April and extended across the central and eastern Pacific, with conditions returning to near normal by late autumn. The general weakening of the trade winds across the equatorial Pacific by the end of autumn contributed to the warming of the subsurface in the central to eastern Pacific (see Fig. 7), while early autumn westerly anomalies contributed to warm subsurface anomalies in the western Pacific.

#### Madden-Julian Oscillation

The Madden-Julian Oscillation (MJO) is a tropical atmospheric anomaly which develops in the Indian Ocean and propagates eastwards into the Pacific Ocean (Donald et al. 2004). The MJO takes between 30 to 60 days to reach the western Pacific and has a frequency of 6 to 12 events per year (Donald et al. 2004). When the MJO is in an active phase, it is associated with increased tropical convection. The temporal evolution of tropical convection anomalies along the equator

Fig. 3 Time-longitude section of 850 hPa wind anomalies along the equator 5°S–5°N from December 2008 to June 2009. The contour interval is 2 m s<sup>-1</sup>.

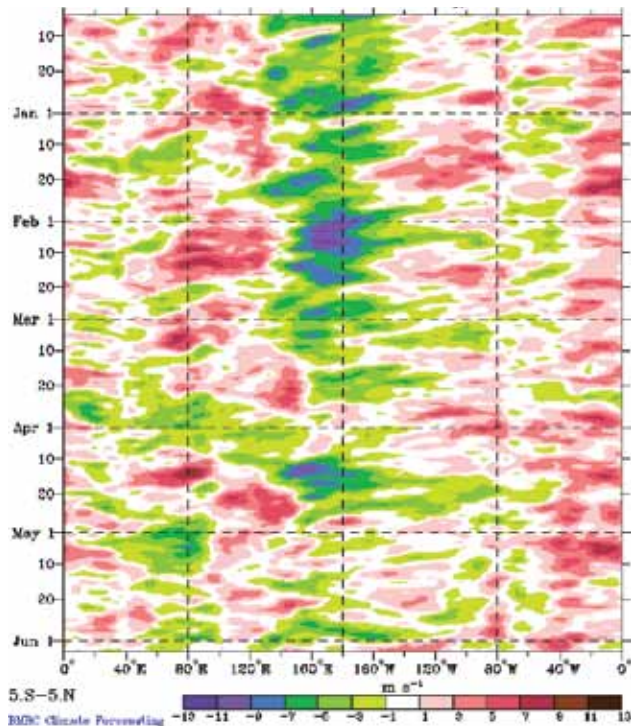
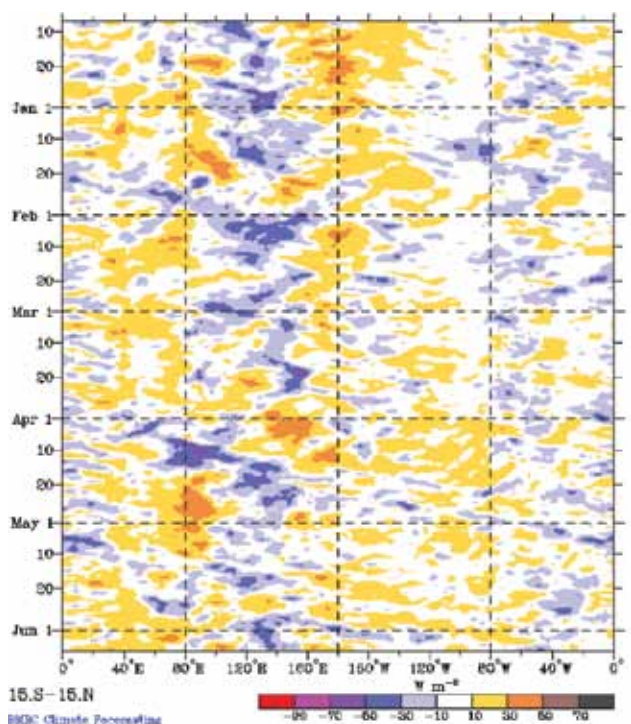


Fig. 4 Time-longitude section of seven-day running mean OLR anomalies ( $W m^{-2}$ ), averaged for 7.5°S–7.5°N, for the period 7 December 2008 to 7 June 2009. The base period is 1979–2001.



tor is shown in Fig. 4, covering the period December 2008 to June 2009. Two eastward-propagating bands of tropical convection are evident through autumn 2009. During early March, the first band of weak MJO-related convection was located in the western Indian Ocean. By the end of March, the band had traversed the Indian Ocean and weakened over the Australian region.

The second band of MJO-related convection was located in the Indian Ocean during mid April. This band moved eastwards towards Australia, weakened and became indiscernible by May. The two MJO events were notable due to their unusually weak penetration across the Australian region which may be associated with the anomalously warm waters in the eastern Indian Ocean.

## Oceanic patterns

### Sea-surface temperatures

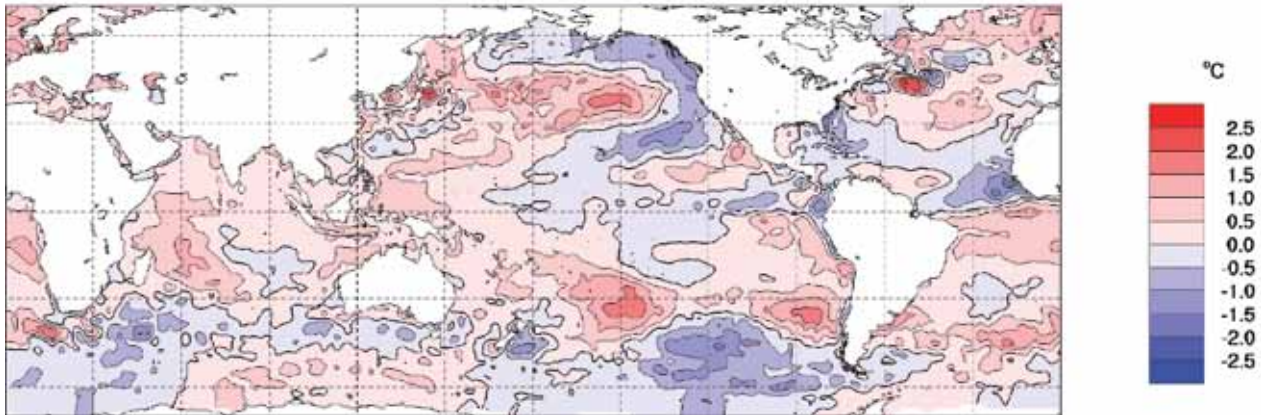
Autumn 2009 sea-surface temperature (SST) anomalies are shown in Fig. 5, obtained from the US National Oceanic and Atmospheric Administration Optimum Interpolation analysis (Reynolds et al. 2002). Positive (warm) anomalies are shown in red shades, and negative (cool) anomalies in blue shades.

In general, the seasonal SST along the equator in the Pacific warmed in autumn, after cooling through the summer months (Mullen 2009), particularly in the central Pacific. By April equatorial waters were neutral, with the exception of persistent early autumn warming between the equator and 30°S off the South American coast. This warming trend continued into May in the eastern Pacific with warm anomalies of 1°C there. This pattern of warming in the eastern Pacific has the spatial characteristics often associated with a developing El Niño, with the exception of the unusual warming evident in the far west of the western Pacific, the Coral Sea and waters off Australia's northern coasts.

The monthly NINO indices (obtained from the National Meteorological and Oceanographic Centre monthly analyses) reflect the transition towards an El Niño event. The NINO3 values (eastern equatorial Pacific) for March, April and May were -0.43, +0.20 and +0.53°C respectively, while the corresponding values for NINO3.4 (central equatorial Pacific) were -0.37, -0.03 and +0.34°C, and for NINO4 (western equatorial Pacific), -0.21, +0.06, and 0.35°C. The rise, particularly in the NINO3 values, over autumn reflected the change from the slightly cool eastern Pacific in late summer to distinct warming off the coast of South America which first appeared in April and began propagating across the Pacific. The April value of the NINO4 index was the first positive monthly value since August 2007.

The Indian Ocean during autumn was in a weakly positive phase, with anomalies mostly in the +0.1°C to +0.7°C range as measured by the Dipole Mode Index (Saji et al. 1999). The index measures the difference in SST anomaly between the tropical west and east of the Indian Ocean; a positive phase often results in a decrease of rainfall over parts of central and southern Australia. Unusually for a positive event, the

Fig. 5 Global anomalies of SST for autumn 2009 (°C). The contour interval is 0.5°C. The base period is 1961-1990.



eastern pole of the IOD was anomalously warm, linking to the warm waters over the western Pacific. The breadth of the warm anomalies over both the equatorial Indian and Pacific Oceans are evident in Fig. 5.

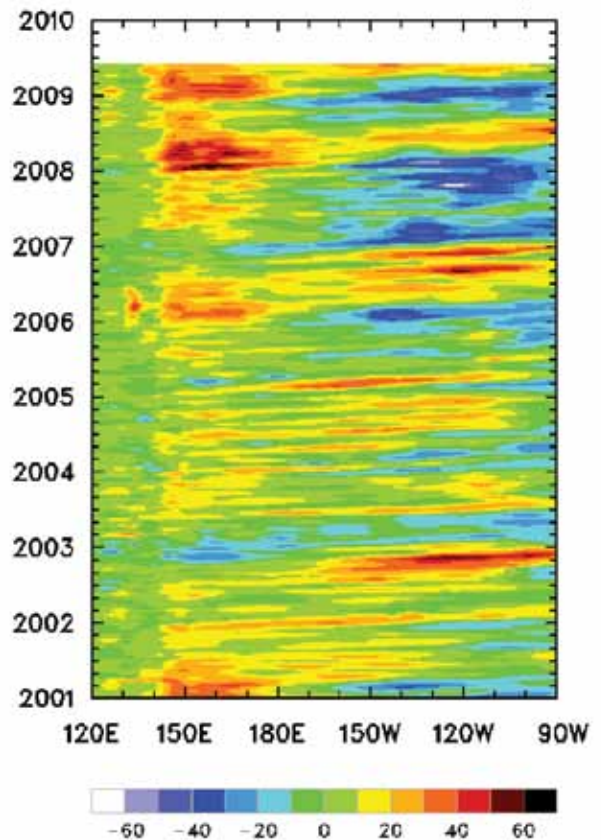
**Subsurface ocean patterns**

A Hovmöller diagram for the 20°C isotherm depth anomaly across the equator from January 2001 to May 2009, obtained from the Centre for Australian Weather and Climate Research (CAWCR), is shown in Fig. 6. The 20°C isotherm depth is generally situated close to the equatorial ocean thermocline, the region of greatest temperature gradient with depth and the boundary between the warm near-surface and cold deep ocean water. Positive anomalies correspond to the 20°C isotherm being deeper than average, and negative anomalies to it being shallower than average. Changes in the thermocline depth may act as a precursor to subsequent changes at the surface.

Negative anomalies dominated the subsurface in the eastern Pacific during summer 2008/09 and these persisted into early autumn. There is evidence of a weak downwelling Kelvin wave progressing eastward throughout autumn, reaching the South American coast in April; this rapidly transitioned the equatorial Pacific from neutral into a weak warm state. The negative subsurface temperatures from summer were replaced by positive anomalies in the eastern equatorial Pacific, along with positive SST anomalies in this region.

The oceanic downwelling Kelvin wave is also observed in the cross-section of the equatorial Pacific temperature anomaly profile (Fig. 7), which shows temperatures down to 400 metres for the months February to May 2009. Red shades indicate positive anomalies (downwelling), and blue shades negative anomalies (upwelling). In profile, the downwelling wave which initiated in summer is evident. This

Fig. 6 Time-longitude section of the monthly anomalous depth of the 20°C isotherm at the equator from 2001 to May 2009. The contour interval is 10 m.



wave strengthened on the thermocline in March and April propagating eastward. By May any lingering regions of negative temperature anomalies from summer in the equatorial Pacific had dissipated.

Fig. 7 Four month, February to May 2009, sequence of vertical temperature anomalies at the equator for the Pacific Ocean. The contour interval is 0.5°C.

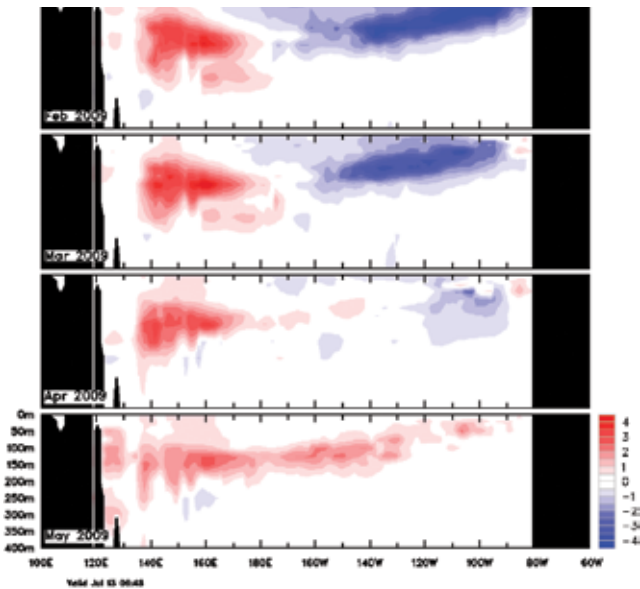


Fig. 8 Southern hemisphere autumn 2009 MSLP (hPa). The contour interval is 5 hPa.

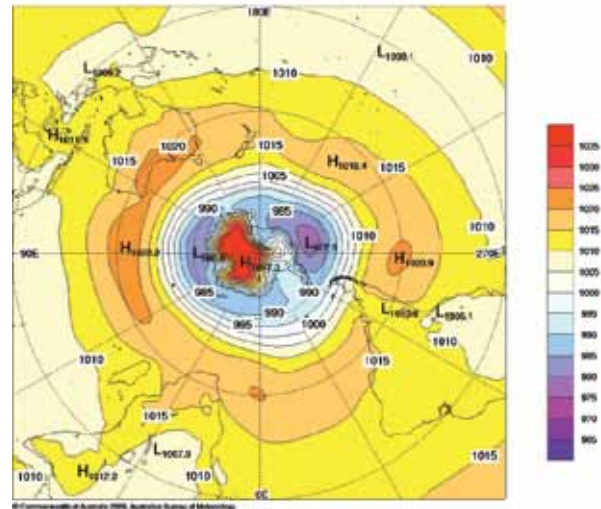
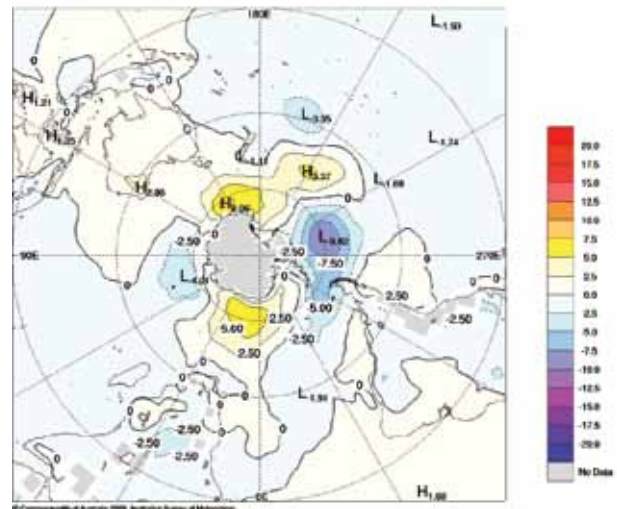


Fig. 9 Southern hemisphere autumn 2009 MSLP anomalies (hPa). The contour interval is 2.5 hPa.



## Atmospheric patterns

### Surface analyses

The southern hemisphere autumn 2009 MSLP pattern, computed from the Bureau of Meteorology’s Global Assimilation and Prognosis (GASP) model, is shown in Fig. 8, with the associated anomaly pattern shown in Fig. 9. These anomalies are the difference from a 1979-2000 climatology obtained from the National Centers for Environmental Prediction (NCEP) II Reanalysis data (Kanamitsu et al. 2002). The MSLP analysis has been computed using data from the 0000 UTC daily analyses of the GASP model. The MSLP anomaly field is not shown over areas of elevated topography (grey shading).

The autumn MSLP pattern in the mid to high latitudes was distinctly zonal in structure. MSLP was generally higher than normal over the Antarctic region, with the exception of south of South America, a region between 60°E and 90°E, and a small region near the date-line to the east of New Zealand. There were two centres in the polar trough around the Antarctic continent, located at 90°E and 100°W. The subtropical ridge was evident in the Australian region, with a centre of high pressure of 1022 hPa over southern Australia.

The Southern Annular Mode (SAM) describes the periodic (ten-day) oscillation of atmospheric pressure between polar and mid-latitude regions of the southern hemisphere. Positive phases of SAM describe increased mass over the extratropics, decreased mass over Antarctica and enhanced mid-latitude westerly flow that is contracted poleward. Conversely, negative phases of SAM describe increased mass over Antarctica, reduced mass over the extratropics and weakened meridional circulation that is expanded equatorward.

The US Climate Prediction Center’s standardised monthly SAM index<sup>3</sup> (Climate Prediction Center 2009) concluded an eleven-month sequence of positive values with a value of -0.73 in May. Due to the transitional nature of SAM during this period, when averaged over the three months there was no significant impact upon the Australian region in terms of pressure or rainfall anomalies (see below). However, above average rainfall was recorded in western Tasmania in May, possibly associated with the negative SAM. Braganza (2008) has identified western Tasmania as having a high correlation between high rainfall and negative SAM events, although it is worth noting other regions which show similar associations to SAM recorded below average rainfall.

<sup>3</sup> This index is derived from daily 700 hPa height anomalies south of 20°S.

**Mid-tropospheric analyses**

The 500 hPa geopotential height (an indicator of the steering of surface synoptic systems) across the southern hemisphere is shown in Fig. 10, with the associated anomalies shown in Fig. 11. Figure 10 shows the autumn 500 hPa height pattern, which, like the MSLP pattern (Fig. 8), displays a zonal structure in the mid to high latitudes. An interesting feature is a divergence in flow evident over and to the east of New Zealand producing a centre of negative anomalies. A comparison of Figs 9 and 11 indicates barotropic pressure anomalies throughout the southern hemisphere.

Fig. 10 Southern hemisphere autumn 2009 500 hPa mean geopotential height (gpm). The contour interval is 100 gpm.

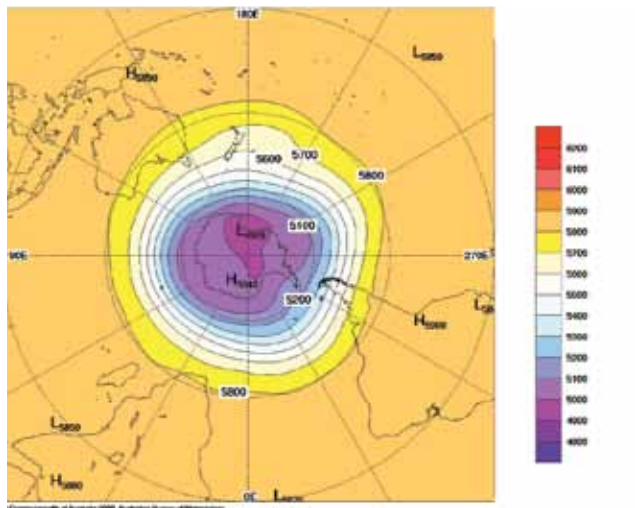
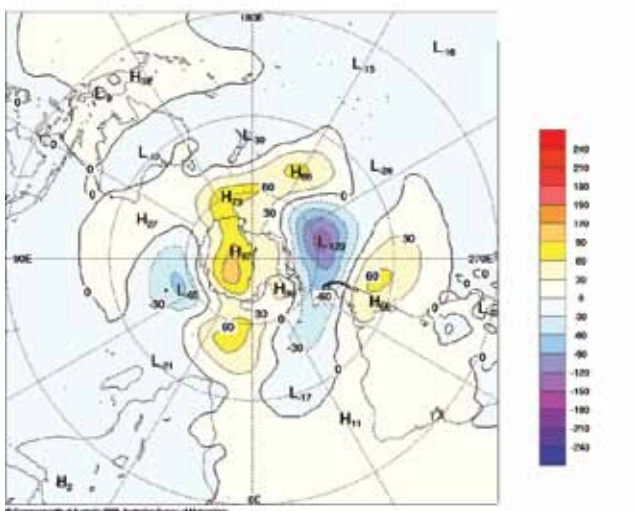


Fig. 11 Southern hemisphere autumn 2009 500 hPa mean geopotential height anomaly (gpm). The contour interval is 30 gpm.



**Blocking**

The time-longitude section of the daily southern hemisphere blocking index (BI)<sup>4</sup> is shown in Fig. 12, with the start of the season at the top of the figure. This index is a measure of the strength of the zonal 500 hPa flow in mid-latitudes relative to that at lower and higher latitudes. Positive values of the blocking index are generally associated with a split in the mid-latitude westerly flow centred near 45°S, and mid-latitude blocking activity.

Fig. 12 Autumn 2009 daily blocking index time-longitude section. The horizontal axis shows degrees east of the Greenwich meridian. Day 1 is 1 March 2009.

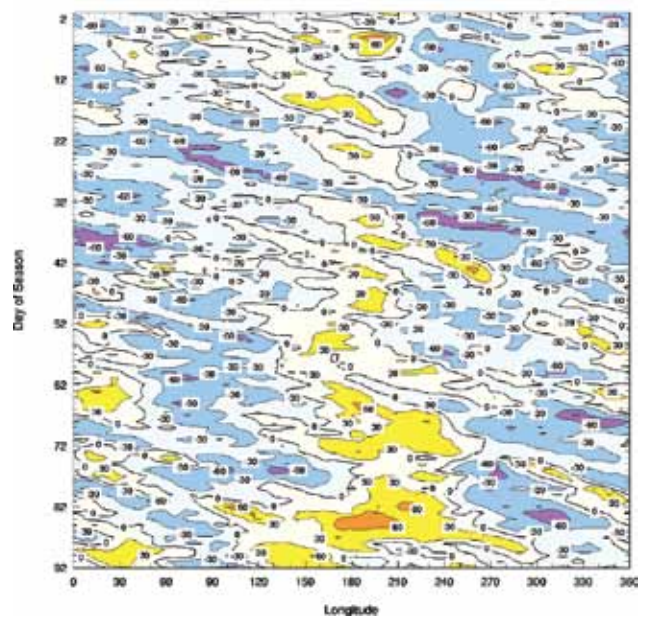
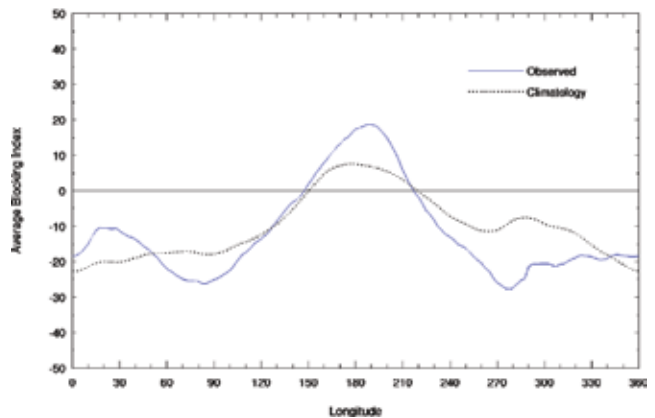
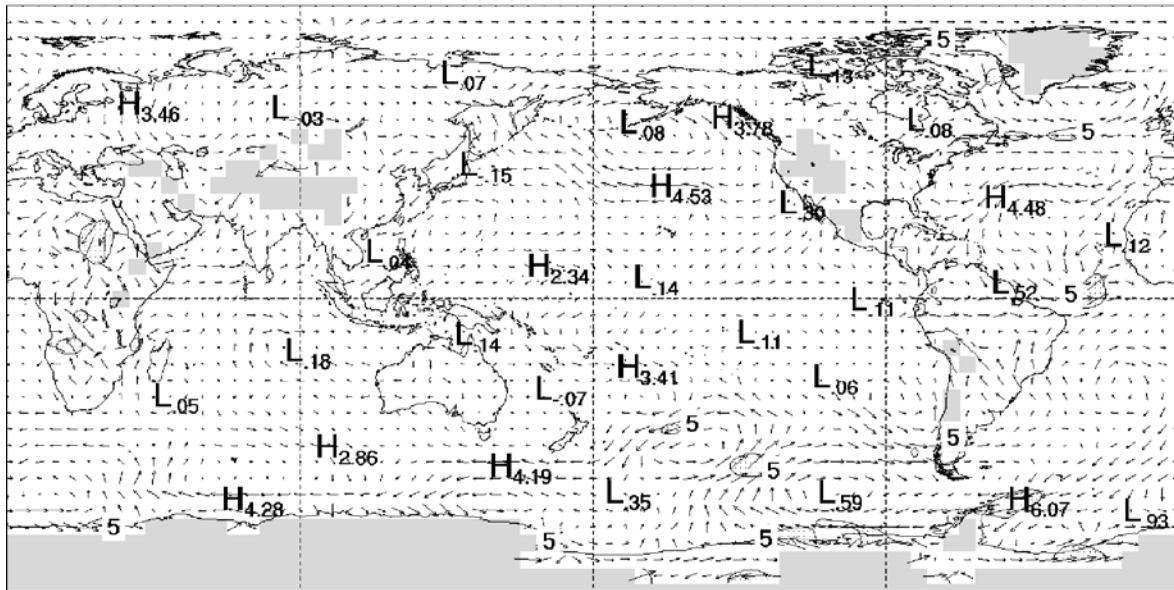
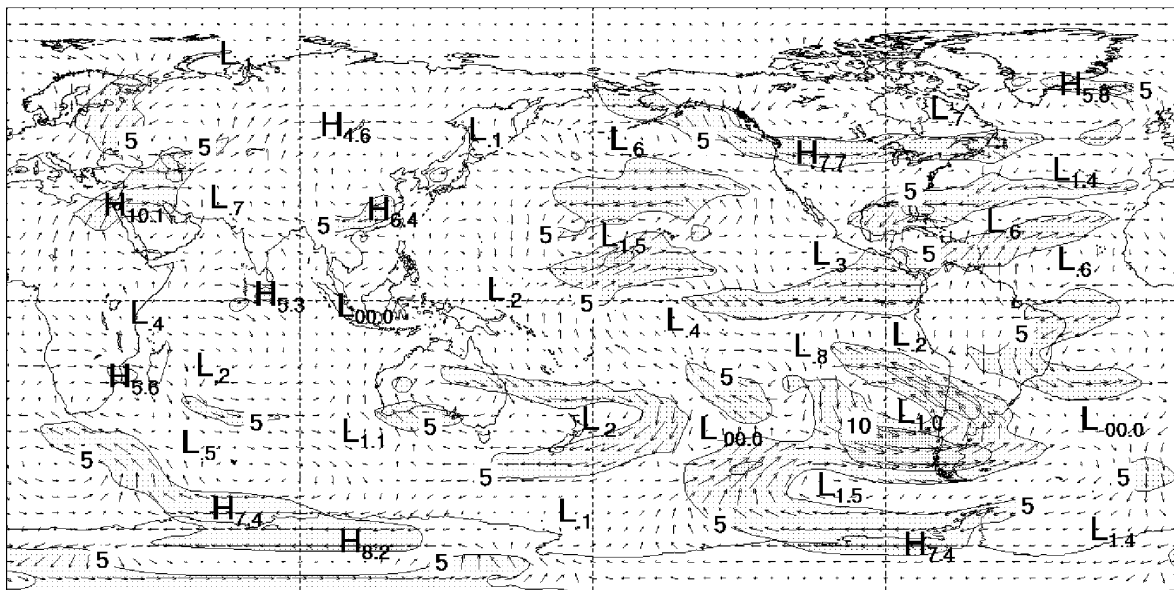


Fig. 13 Mean southern hemisphere blocking index for autumn 2009 (solid line). The dashed line shows the corresponding long-term average. The horizontal axis shows degrees east of the Greenwich meridian.



<sup>4</sup> The blocking index is defined as  $BI = 0.5[u_{25} + u_{30} - (u_{40} + 2u_{45} + u_{50}) + u_{55} + u_{60}]$  where  $u_x$  is the zonal (east-west) component of the 500 hPa wind at latitude  $x$ .

Fig. 14 Global autumn 2009 850 hPa vector wind anomalies ( $\text{m s}^{-1}$ ).Fig. 15 Global autumn 2009 200 hPa vector wind anomalies ( $\text{m s}^{-1}$ ).

Blocking activity oscillated across Australian longitudes ( $120^{\circ}\text{E}$  to  $180^{\circ}$ ) during autumn, with positive anomalies dominating towards the end of May. Figure 13, which shows the seasonal index for each longitude, indicates below average blocking is a dominant feature at longitudes on either side of the Australian region.

Peak seasonal mean BI values were located at  $170^{\circ}\text{W}$ , close to the region of maximum climatological values. The region from eastern Australia to the central Pacific,  $40^{\circ}\text{E}$  to  $140^{\circ}\text{W}$ , is climatologically favoured for blocking (Trenberth and Mo 1985; Sinclair 1996). Two distinct blocking minima at  $80^{\circ}\text{E}$  and  $80^{\circ}\text{W}$  are evident in Fig. 11, particularly during the end of March and early April.

### Winds

Autumn 2009 low-level (850 hPa) and upper-level (200 hPa) wind anomalies (from the 22-year NCEP II climatology) are shown in Figs 14 and 15, respectively. Isotach contours are at  $5 \text{ m s}^{-1}$  intervals, and in Fig. 14, regions where the surface rises above the 850 hPa level are shaded.

Low-level trade wind flow was near normal across the Pacific in autumn with enhanced flow near the South American coast. Over the tropical central and eastern Pacific, westerly flow dominated in the upper levels, with the strongest anomalies observed in the eastern Pacific.

In the Australian region low-level flow was near normal over eastern Australia, with weak northerly dominated flow

over central Australia and easterly flow over western Australia. At upper levels, anomalous cyclonic flow was centred to the east of Australia, with the strongest southerly anomalies over western Australia, westerly flow over northern Australia and southerly flow over eastern Australia. This was consistent with the weak pressure anomalies covering much of the continent and slightly below to near normal rainfall over most of the continent.

## Australian Region Climate

### Rainfall

Australian rainfall totals for autumn are shown in Fig. 16, while the rainfall deciles for the same period are shown in Fig. 17. Rainfall deciles are calculated using all autumns from 1900 to 2009.

Rainfall was below to very much below average in the west and southwest of Western Australia (including the Kimberley and parts of the west Pilbara, and Gascoyne south through to the Southwest Land Division), and also across much of the tropical north of the country (Fig. 17) although this is a relatively seasonally dry period in those parts. 22.2% of Western Australia (WA) and 25.6% of the Northern Territory (NT) recorded very much below average (decile 1) rainfall in autumn, with 11.7% and 13.5%, respectively, recording seasonal rainfalls below the 5th percentile. Several small regions in WA, including one immediately to the south of Perth, saw record low autumn rainfalls.

Only small parts of Australia were wetter than normal during autumn 2009; the mid-north coast of New South Wales (NSW) through to the southeast coast of Queensland (Qld) experienced very much above average rainfall for the season, particularly related to heavy rainfall events in May, with seasonal totals approaching double the long-term average. Parts of central and western South Australia (SA), western Tasmania (Tas.) and a small part of northwest Western Australia also experienced above average rainfall.

In area-averaged terms the season ranked 14th lowest out of the 110 autumns between 1900 and 2009 nationally, and was 41% below the 1961-1990 mean. All States and the Northern Territory recorded area-averaged seasonal totals which were below the 1961-1990 mean, although for two of them (NSW and SA) these outcomes were still above the long-term (1900-2009) median.

The national highest 24-hour rainfall total for the autumn season was 510 mm recorded on 1 April at Urunga in NSW (Table 1). The highest seasonal rainfall total was 2417 mm at Bellenden Ker Top Station in Queensland.

### Drought

At the end of autumn, 13.1% of Australia was in serious rainfall deficiency (decile 1) for the three months ending May 2009. As previously noted, this area comprised 25.6% of the NT and 22.2% of WA, with an additional 5.1% each of Victoria and Queensland. For this period, 6.7% of the country was in severe deficiency (below the 5th percentile).

Fig. 16 Autumn 2009 rainfall totals (mm) for Australia.

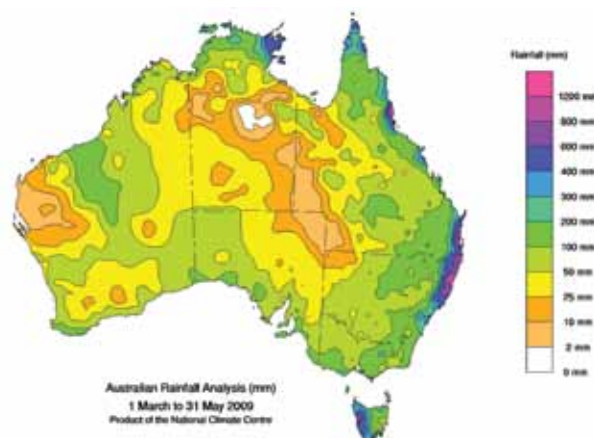
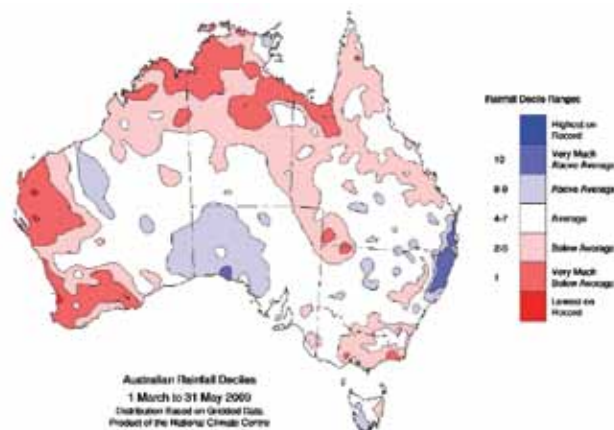


Fig. 17 Autumn 2009 rainfall deciles. Deciles based on grid-point values over the autumns 1900 to 2009.



For shorter and longer drought assessment periods, the total national area in serious rainfall deficiency was less than this local temporal maximum, with another local temporal maximum at a period length of 24 months ending May 2009, in which 10.0% of the country was in serious rainfall deficiency (with 4.2% in severe rainfall deficiency). For this longer period, the main regions affected were Victoria (70.0%), Tasmania (56.1%), SA (24.7%), NSW (11.0%) and the NT (10.5%).

### Temperatures

Figures 18 and 19 show maximum and minimum temperature anomalies for autumn, while temperature deciles are shown in Fig. 20 for maximum temperature and Fig. 21 for minimum temperature. Seasonal anomalies are calculated with respect to the 1961-1990 period using all stations for which a 1961-1990 normal is available. The deciles (Figs 20 and 21) and areal averages (Tables 2 and 3) are calculated from monthly analyses using a high-quality subset of the temperature network.

Table 1. Summary of the seasonal rainfall ranks and extremes on a national and State basis for autumn 2009.

	Highest seasonal total (mm)	Lowest seasonal total (mm)	Highest 24 hour fall (mm)	Area-averaged rainfall (AAR) (mm)	Rank of AAR *
Australia	2417 at Bellenden Ker Top Station (Qld)	Zero at several locations	510 at Urunga (NSW), 1 April	71.0	14
WA	230 at Wereroa	Zero at several locations	137 at Marble Bar, 1 March	48.7	15
NT	761 at Nhulunbuy	Zero at Brunchilly Station	153 at Cape Wessel, 5 May	52.1	12
SA	363 at Mt Lofty Botanic Garden	3 at Clifton Hills Station	77 at Turkey Lane, 25 May	49.1	67
Qld	2417 at Bellenden Ker Top Station	Zero at several locations	464 at Black Pinch Road (Noosa River), 3 April	89.5	20
NSW	1807 at Promised Land	2 at Barrona Downs Station	510 at Urunga, 1 April	126.9	71
Vic.	492 at Weeaprounah	39 at Pirlita	80 at Mt Buffalo Chalet, 25 April	106.9	27
Tas.	1175 at Mt Read	60 at Swansea	141 at Mt Read, 15 May	326.9	53

\* The rank goes from 1 (lowest) to 110 (highest) and is calculated over the years 1900 to 2009 inclusive.

Fig. 18 Autumn 2009 maximum temperature anomalies (°C) for Australia: anomalies based on a 1961-1990 mean.

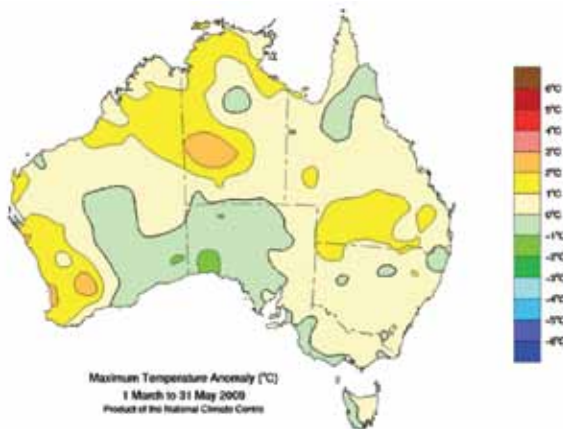


Fig. 20 Autumn 2009 maximum temperature deciles for Australia. Deciles based on grid-point values over the autumns 1950 to 2009.

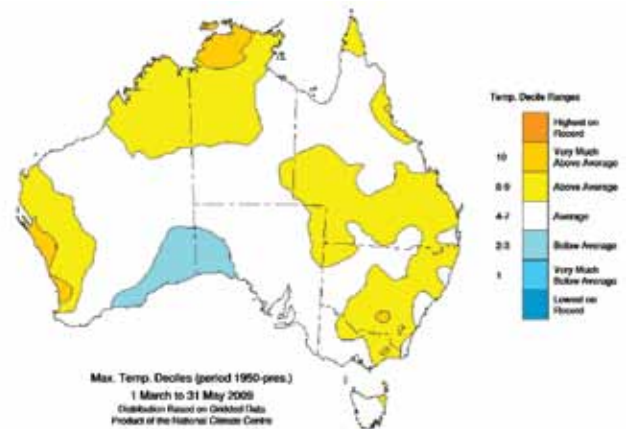


Fig. 19 Autumn 2009 minimum temperature anomalies (°C) for Australia: anomalies based on a 1961-1990 mean.

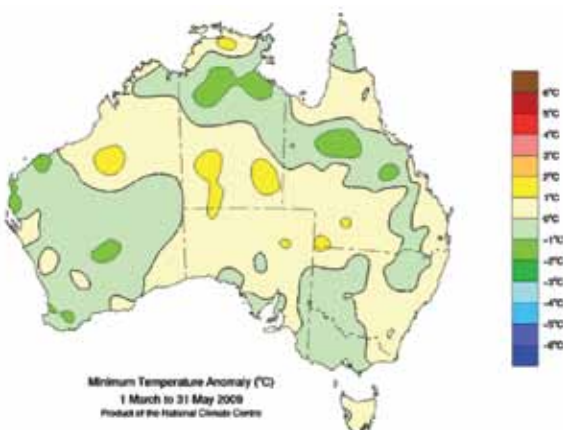


Fig. 21 Autumn 2009 minimum temperature deciles for Australia. Deciles based on grid-point values over the autumns 1950 to 2009.

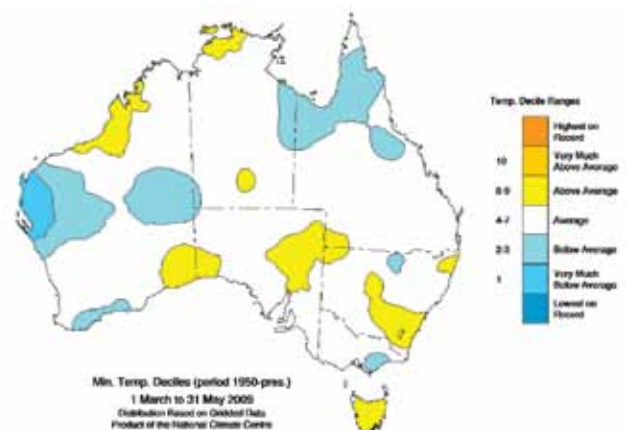


Table 2. Summary of the seasonal maximum temperature ranks and extremes on a national and State basis, for autumn 2009.

	<i>Highest seasonal mean (°C)</i>	<i>Lowest seasonal mean (°C)</i>	<i>Highest daily recording (°C)</i>	<i>Lowest daily recording (°C)</i>	<i>Anomaly of area-averaged mean (°C) (AAM)</i>	<i>Rank of AAM*</i>
Australia	36.7 at Wyndham (WA)	8.1 at Mt Wellington (Tas.)	45.2 at Moomba (SA), 3 March	-2.8 at Mt Hotham (Vic.), 26 April	+0.51	42
WA	36.7 at Wyndham	21.0 at Albany	44.5 at Onslow, 28 March	10.3 at Rocky Gully, 22 May	+0.46	39/40
NT	36.1 at Bradshaw	27.4 at Kulgera	42.5 at Walungurru, 23 March	9.0 at Kulgera, 30 May	+0.72	44
SA	29.2 at Moomba	15.4 at Mount Lofty	45.2 at Moomba, 3 March	8.1 at Mt Lofty, 29 May	+0.01	28
Qld	33.9 at Century Mine and Normanton	21.1 at Applethorpe	44.8 at Birdsville, 3 March	12.0 at Applethorpe, 20 and 21 May	+0.68	46/47
NSW	29.0 at Mungindi	8.7 at Thredbo Top Station	44.7 at Tibooburra, 3 March	-2.7 at Thredbo Top Station, 26 April	+0.61	45/47
Vic.	23.9 at Mildura	8.5 at Mt Hotham	38.5 at Hopetoun, 21 March	-2.8 at Mt Hotham, 26 April	+0.28	40
Tas.	19.3 at Launceston	8.1 at Mt Wellington	30.5 at Ouse, 21 March	-1.9 at Mt Wellington, 27 April	+0.12	37

\* The temperature ranks go from 1 (lowest) to 60 (highest) and are calculated over the years 1950 to 2009 inclusive. Multiple ranks indicate the presence of tied values within the time series.

Table 3. Summary of the seasonal maximum temperature ranks and extremes on a national and State basis, for autumn 2009.

	<i>Highest seasonal mean (°C)</i>	<i>Lowest seasonal mean (°C)</i>	<i>Highest daily recording (°C)</i>	<i>Lowest daily recording (°C)</i>	<i>Anomaly of area-averaged mean (°C) (AAM)</i>	<i>Rank of AAM*</i>
Australia	27.3 at Troughton Island (WA)	-1.0 at Charlotte Pass (NSW)	31.2 at Birdsville, (Qld) 2 March	-13.0 at Charlotte Pass (NSW), 29 April	-0.02	33/34
WA	27.3 at Troughton Island	7.4 at Collie East	30.1 at Roebourne, 3 April	-1.4 at Eyre, 29 May	-0.16	26
NT	25.9 at McCluer Island	13.1 at Kulgera	29.6 at Alice Springs, 3 March	2.8 at Kulgera, 12 May	+0.11	36
SA	15.9 at Moomba	7.8 at Coonawarra	30.2 at Moomba, 3 March	-0.7 at Naracoorte, 30 May	+0.37	39
Qld	24.9 at Horn Island	9.5 at Stanthorpe	31.2 at Birdsville, 2 March	-4.0 at Stanthorpe, 15 May	-0.19	29
NSW	17.0 at Yamba	-1.0 at Charlotte Pass	26.8 at Tibooburra, 3 March	-13.0 at Charlotte Pass, 29 April	+0.12	39
Vic.	13.9 at Gabo Island	2.3 at Mt Hotham	21.7 at Melbourne Airport, 3 April	-8.2 at Mt Hotham, 29 April	-0.39	31
Tas.	12.7 at Hogan Island	2.2 at Mt Wellington	19.7 at Flinders Island, 22 March	-7.5 at Liawenee, 29 April	+0.45	51/53

\* The temperature ranks go from 1 (lowest) to 60 (highest) and are calculated over the years 1950 to 2009 inclusive. Multiple ranks indicate the presence of tied values within the time series.

Seasonal minimum temperatures for autumn 2009 were within 1°C of average across most of the country. Scattered small regions with anomalies in the -1 to -2°C range were seen in Qld, NT and WA, with scattered small regions with anomalies in the +1 to +2°C range lying in a band running

from west to east across central Australia (WA, southern NT, northern SA, southwest Queensland and northwest NSW). Nationally, the areally averaged autumn minimum temperature was -0.02°C, with Tasmania being the warmest State in relative terms (+0.45°C; 9th warmest autumn in a three-way

tie with 2003 and 1971) and Victoria the coldest ( $-0.39^{\circ}\text{C}$ ). Minimum temperatures were very much below average (decile 1) in far western WA, around Shark Bay (Fig. 21). The highest daily recorded minimum temperature was  $31.2^{\circ}\text{C}$  at Birdsville in Queensland on 2 March. The lowest daily minimum temperature was  $-13.0^{\circ}\text{C}$  on 29 April, and the lowest seasonal mean minimum temperature was  $-1.0^{\circ}\text{C}$ , both recorded at Charlotte Pass in NSW (Table 3).

## References

- Braganza, K. 2008. Seasonal climate summary southern hemisphere (autumn 2007): La Niña emerges as a distinct possibility in 2007. *Aust. Met. Mag.*, 57, 65-75.
- Climate Diagnostics Center 2009a. Numerical values of the MEI time series since 1950. <http://www.cdc.noaa.gov/people/klaus.wolter/MEI/table.html>.
- Climate Diagnostics Center 2009b. Historical ranks of the MEI. <http://www.cdc.noaa.gov/people/klaus.wolter/MEI/rank.html>
- Climate Prediction Center 2009. Monthly mean AAO index since January 1979. [http://www.cpc.noaa.gov/products/precip/CWlink/daily\\_ao\\_index/aa0/aa0.shtml](http://www.cpc.noaa.gov/products/precip/CWlink/daily_ao_index/aa0/aa0.shtml).
- Donald, A., Meinke, H., Power, B., Wheeler, M. and Ribbe, J. 2004 Forecasting with the Madden-Julian Oscillation and the applications for risk management. In: *4th International Crop Science Congress*, 26 September - 01 October 2004, Brisbane, Australia.
- Kanamitsu, M., Ebisuzaki, W., Woollen, J., Yang, S.-K., Hnilo, J. J., Fiorino, M. and Potter, G. L. 2002. NCEP-DOE AMIP-II Reanalysis (R-2). *Bull. Am. Met. Soc.*, 83, 1631-43.
- Mullen, C. 2009. Seasonal climate summary southern hemisphere (summer 2008-09): a weak, brief La Niña returns. Bumper wet season in tropical Australia; exceptional heatwaves in southeastern Australia. *Aust. Met. Oceanogr. J.*, 58, 275-84.
- Reynolds, R.W., Rayner, N.A., Smith, T.M., Stokes, D.C. and Wang, W. 2002. An improved in situ and satellite SST analysis for climate. *Jnl Climate*, 15, 1609-25.
- Saji, N.H., Goswami, B.N. Vinayachandran, P.N. and Yamagata, T. 1999. A dipole mode in the tropical Indian Ocean. *Nature*, 401, 360-3.
- Sinclair, M.R. 1996. A climatology of anticyclones and blocking for the Southern Hemisphere. *Mon. Weath. Rev.*, 124, 245-63.
- Trenberth, K. and Mo, K.C. 1985. Blocking in the Southern Hemisphere. *Mon. Weath. Rev.*, 113, 3-21.
- Troup, A.J. 1965. The Southern Oscillation. *Q. Jl R. Met. Soc.*, 91, 490-506.
- Vincent, D.G., Fink, A., Schrage, J.M. and Speth, P. 1998. High-and-low frequency intraseasonal variance of OLR on annual and ENSO timescales. *Jnl Climate*, 11, 968-86.
- Wolter, K. and Timlin, M.S. 1993. Monitoring ENSO in COADS with a seasonally adjusted principal component index. *Proc. of the 17th Climate Diagnostics Workshop*, Norman, OK, NOAA/NMC/CAC, NSSL, Oklahoma Clim. Survey, CIMMS and the School of Meteorology, Univ. of Oklahoma, 52-7.
- Wolter, K. and Timlin, M.S. 1998. Measuring the strength of ENSO – how does 1997/98 rank? *Weather*, 53, 315-24.

